To appear in Astrophysical Journal
Preprint typeset using LaTeX style emulateapj v. 11/12/01

UNRAVELLING THE PUZZLE OF THE ECLIPSING POLAR SDSSJ 015543.40+002807.2 WITH *XMM* AND OPTICAL PHOTOMETRY/SPECTROPOLARIMETRY[1]

Gary D. Schmidt[2], Paula Szkody[3], Lee Homer[3], Paul S. Smith[2], Bing Chen[4], Arne Henden[5], Jan-Erik Solheim[6], Michael A. Wolfe[3], and Robert Greimel[7]

To appear in Astrophysical Journal

ABSTRACT

The cataclysmic variable SDSSJ 015543.40+002807.2 is confirmed to be a magnetic system of the AM Herculis type. With an orbital period of 87.13 minutes, it is also the shortest-period eclipsing Polar known. Monitoring with *XMM-Newton* finds a high-state light curve dominated by a single X-ray emitting accretion pole located slightly prograde of the secondary star. The hard X-ray spectrum is typical of radial shocks on magnetic white dwarfs ($kT \sim 10$ keV), and there is evidence for a soft X-ray component consistent with reprocessing from the stellar surface. The optical circular polarization is weak ($v \lesssim 3\%$) when the accretion rate is high ($m_V \sim 15.5$), due to optically-thick cyclotron emission and the apparent competition between two accreting poles. However, in low states ($m_V \sim 18$), the polarization increases smoothly to the blue, reaching 20% at 4200 Å, and the flux spectrum displays a rich set of thermally-broadened cyclotron harmonics that indicate a polar field of 29 MG. The phase interval preceding the 6.5 min eclipse depicts the development of P-Cygni components followed by complete absorption reversals in the emission lines. This phenomenon is not unexpected for a strongly accreting magnetic system viewed through the cool base of the funnel, and high-quality spectroscopy through this interval will likely lead to new insights into the dynamics of magnetic coupling and gas flow onto the white dwarf.

Subject headings: binaries: spectroscopic — novae, cataclysmic variables — stars: individual (SDSS J015543.40+002807.2) — stars: magnetic fields — X-rays: stars

1. INTRODUCTION

Despite a catalog of nearly 80 systems (e.g., Ritter & Kolb 2003), discoveries of new AM Herculis systems, or Polars, continue to provide insights into the phenomenon of accretion onto compact magnetic objects through the exploration of interesting geometries and new regions of parameter space. For example, we have only recently begun to appreciate the degree that a very strong field ($B \gtrsim 100$ MG) on the white dwarf primary star reduces the observed circular polarization – the hallmark of strongly magnetic cataclysmic variables (mCVs) – by shifting the higher optical-depth, low-harmonic cyclotron emission features into the optical portion of the spectrum (Schmidt et al. 1996; 2001). Unusually high specific mass-transfer rates ($\dot{m} \gtrsim 10$ g cm^{-2} s^{-1}) can depress the accretion spot below the surrounding photosphere, and thereby also yield low polarization (e.g., Stockman 1988). By contrast, very low-$\dot{m}$ systems ($< 10^{-2}$ g cm^{-2} s^{-1}) have begun to appear in deep spectroscopic surveys (Reimers, Hagen, & Hopp, 1999; Reimers & Hagen 2000; Szkody et al. 2003), where the reduced Doppler broadening and high contrast to underlying sources of emission give rise to striking cyclotron harmonic features that can be mistaken for quasar emission lines. Due to the low optical depth, circular polarization in these features can exceed 70%.

Eclipsing geometries are particularly valuable for all binary types because the transition timings and profiles allow the locations and sizes of emission regions to be mapped within the systems. The accretion binary SDSS J015543.40+002807.2 (hereafter SDSS J0155+0028) was discovered by Szkody et al. (2002) in the Early Release Data of the Sloan Digital Sky Survey (SDSS). The SDSS spectrum was saturated due to its brightness, but follow-up time-resolved spectroscopy with the Apache Point Observatory in November 2000 showed strong He II λ4686 emission and a large amplitude radial velocity curve with an orbital period of 87 min. The most intriguing aspect of the system was that the Balmer and He I (but not the He II) emission lines went into absorption for part of the orbit, while the continuum did not change during those phases. In addition, the phasing of the absorption did not correspond to the spectroscopic zero-crossing of the radial velocities, such as would result from an eclipse of the white dwarf by the secondary star. SDSS J0155+0028 was also weakly detected in *ROSAT* survey observations. Based

[1] Some of the results presented here were obtained with the MMT Observatory, a facility operated jointly by The University of Arizona and the Smithsonian Institution. Additional results are based on observations made with the Nordic Optical Telescope, operated on the island of La Palma jointly by Denmark, Finland, Iceland, Norway, and Sweden, in the Spanish Observatorio del Roque de los Muchachos of the Instituto de Astrofisica de Canarias.

[2] Steward Observatory, The University of Arizona, Tucson AZ 85721; gschmidt@as.arizona.edu, psmith@as.arizona.edu

[3] Department of Astronomy, University of Washington, Box 351580, Seattle, WA 98195-1580; szkody@astro.washington.edu, homer@astro.washington.edu, maw2323@u.washington.edu

[4] XMM-Newton Science Operations Centre, ESA/Vilspa, 28080, Madrid, Spain, bchen@xmm.vilspa.esa.es

[5] Universities Space Research Association/US Naval Observatory, Flagstaff Station, P.O. Box 1149, Flagstaff, AZ 86002-1149; aah@nofs.navy.mil

[6] Institute of Theoretical Astrophysics, P.O. Box 1029, Blindern, Oslo, N-0315, Norway, j.e.solheim@astro.uio.no

[7] ING, Apartado de Correos, 321, 38700 Santa Cruz de La Palma, Canary Islands, Spain, greimel@ing.iac.es

on these characteristics, the system was proposed to be a likely high inclination mCV. If found to be strongly polarized, SDSS J0155+0028 would be the shortest-period eclipsing AM Her system known.

Optical photometry obtained when the system was bright ($m_V \approx 15.2$) by students at the Nordic-Baltic Research Course (Dubkova, Kudryavtseva & Hirv 2003) in 2002 August supported this picture by revealing a deep (5.9 mag), narrow (∼400 s) eclipse superposed on a broad hump. This is characteristic of a magnetic accretion system dominated by a single pole in which the accretion spot is self-eclipsed by the white dwarf for less than half the orbital period. Further photometry of SDSS J0155+0028 by Woudt, Warner, & Pretorius (2004) on 2003 October 4−5 found the system in a low accretion state ($m_V \sim 18$) but still strongly variable on a period of 87.13 ± 0.02 min. The brightness hump has a different shape and is narrower in width than in the high state observations.

In this paper we report the results of *XMM-Newton* X-ray and ground-based optical photometry, spectroscopy and spectropolarimetry that confirm SDSS J0155+0028 to be a magnetic CV. The system is characterized by wide swings in mass-transfer rate and an unusual viewing geometry that offers new avenues for studying the structure of accretion columns in Polars.

2. OBSERVATIONS

2.1. *XMM-Newton Observations*

X-ray observations of SDSS J0155+0028 were obtained in a single time series with the *XMM-Newton* Observatory on 2003 July 4 covering 14:27−16:34 UT. Useful data were obtained by each of the EPIC X-ray CCD cameras (EPIC-pn, and the two EPIC-MOS, each of which has about half the effective area of the pn; Turner et al. 2001), using the "Thin1" filter and "Prime Full Window" mode. These data are summarized in Table 1. However, the source was sufficiently faint that neither the continuum nor any bright emission lines were detected with the dispersing reflection grating spectrograph (RGS; den Herder et al. 2001). Moreover, due to a technical failure, no usable time-resolved data were available from the optical monitor (OM; Mason et al. 2001). The data were analyzed following the ABC guide from the *XMM-Newton* US GOF web site[8] and analysis threads from the main Vilspa site[9], employing calibration files current to 2004 March 23 and the SAS v6.0. First, the ODF files were reprocessed to produce new event files. The event list was then screened using the standard expressions and energies were restricted to the range 0.1−10 keV. For the pn, source data were extracted within a 360 pixel radius circular aperture (this only encircles ∼ 70% of the energy, but for low count-rate sources reduces the background contribution) using a background computed from adjacent rectangular regions at similar detector Y locations to the target. As advised, a conservative choice of event selection, pattern = 0, was adopted. For the two MOS detectors, event pattern ≤12 was applied and a 320 pixel aperture size was used (also enclosing ∼70% of the energy), but the background was based on an annulus surrounding the source. We note that the fluxes and count rates quoted in what follows have been corrected for the encircled energy fraction.

Light curves were extracted for both source and background with the SAS task `evselect`, using the same extraction regions as the spectra, but with a less conservative pattern ≤ 4 for the pn events. The task `lccor` was then used to scale the data and achieve background subtraction, dead-time, and vignetting corrections, producing net source light curves with 20 s and 100 s binning. Finally, the time stamps were corrected to the solar system barycenter using FTOOLS tasks (giving HJD(TB)), and then 64.184 s was subtracted to yield HJD(UT) for comparison with the ground-based observations. The 100 s binned light curves for the three detectors are shown in Figure 1. From the PIMMS conversion software available at the NASA HEASARC web site[10], and an input model consisting of an absorbed ($n_H = 2.73 \times 10^{20}$ cm^{-2}), 7 keV thermal bremsstrahlung component, the *XMM* peak count rates of 0.3 c s^{-1} in the MOS telescopes and 0.8 c s^{-1} in the PN (all ∼0.1−10 keV) correspond to ∼0.09 cps with the *ROSAT* PSPC, suggesting that the system was in an active accretion state, comparable to to that during the *ROSAT* observation (0.04 cps).

2.2. *Ground-Based Observations*

Optical photometry was obtained at the United States Naval Observatory (USNO) 1 m telescope with a CCD and V filter on the nights immediately preceding (July 4 UT) and following (July 5 UT) the *XMM* observations, as well as a long sequence on 2002 November 15. Differential photometry was used to construct the light curves shown in Figure 2, which are folded and phased based on the ephemeris described below. While the results indicate that SDSS J0155+0028 may have been ∼1 mag fainter than when measured by Dubkova et al. (2003), they confirm that the system was actively accreting during the period of X-ray monitoring.

Additional CCD photometry during the high state was added to study the eclipse in different filters and to establish the eclipse ephemeris. Differential photometry with respect to the same comparison star listed in Dubkova et al (2003) was obtained with the Manastash Ridge Observatory 0.76 m telescope on 2002 September 14 using a V filter and 15 s exposure times. Differential photometry with a combination of comparison stars using the 2.56 m Nordic Optical Telescope (NOT) on 2002 October 16 provided B light curves with 8.2 s integrations and an R light curve with 7.8 s integrations. On that same night, 30 s integrations without a filter were obtained at the 0.6 m telescope at the Observatorio del Roque de los Muchachos. Further B observations using 27.9 s integrations were also made at the 0.8 m telescope at Observatoria del Teide on 2002 November 14. Figure 3 shows representative light curves in B, V and R filters from these observations and the eclipse timings are given in Table 2. The light curves are fairly similar in the different filters. Only the R filter has the time resolution and signal-to-noise ratio to provide some information on the eclipse shape, indicating that it does

[8] http://heasarc.gsfc.nasa.gov/docs/xmm/abc/abc.html

[9] http://xmm.vilspa.esa.es/external/xmm_sw_cal/sas.shtml

[10] http://heasarc.gsfc.nasa.giv/Tools/w3pimms.html

not appear to have a flat bottom and the egress is steeper than the ingress. Comparing this profile with the V data of Dubkova et al (2003) (both obtained with the NOT), it appears that the eclipse in V is about 2 magnitudes deeper than in R. The other point of note is the presence of a brief but noticeable drop (almost a magnitude) about 0.1 phase prior to the eclipse, which is a prominent feature in B and R (but less so in V) in all data from 2002 August through November. If this feature arises through absorption by the stream (see §5), it is not a permanent feature as it is not apparent in the high state data of 2003 July (Figure 2).

Optical spectrophotometry and circular spectropolarimetry of SDSS J0155+0028 were obtained on 2002 December 5 UT with the 2.3 m Bok telescope of Steward Observatory and again on 2004 February 16 UT with the 6.5 m MMT atop Mt. Hopkins. Both runs made use of the CCD SPOL spectropolarimeter (Schmidt, Stockman, & Smith 1992), configured for broad spectral coverage ($\lambda\lambda 4200-8200$) at a rather low resolution of $\sim$15 Å. In 2003 the instrument was upgraded with a cosmetically perfect, $1200\times800\times15$ μm pixel CCD from Semiconductor Technology Associates, Inc. that was thinned, antireflection-coated, and permanently sensitized through backside charging at the Steward Observatory Imaging Technology Laboratory. The time series spectropolarimetry used an exposure of 240 s per observation for an effective time resolution of $\Delta\varphi \sim 0.065$. Total flux spectra are recorded at twice this frequency. The 2002 Dec. observations found SDSS J0155+0028 in a high accretion state, with $m_B = 15.1$ at maximum brightness and $\sim$20 at mid-eclipse. This data series is also the more extensive, covering 1.5 orbital periods (and 2 eclipses). The 2004 Feb. observations were obtained as the object set in evening twilight, so were limited to only slightly more than a quarter of the orbital period. From the comparison of spectrum-added circular polarization and B-band brightness shown in Figure 4, it is clear that SDSS J0155+0028 was in a much lower accretion state at this epoch, with $m_B > 18$ and fading through the sequence. Again, phasing was accomplished using the ephemeris derived below. Note the general similarities between the two panels of Figure 4, notably the rapid drop in brightness between $\varphi = 0$ and 0.3 that has been seen at all epochs to date (e.g., Figures 2 and 3; Dubkova et al. 2003; Woudt et al. 2004), and the same sign of circular polarization in this phase interval (see also below).

3. HIGH STATE X-RAY LIGHT CURVE AND SPECTRUM

Both the X-ray and contemporaneous optical photometric light curves show a single bright phase, punctuated near the middle by a virtually total eclipse of duration $\sim$390 s ($\Delta\varphi \sim 0.075$). This is best seen in the light curve obtained by summing the two MOS detectors and folding on the orbital period, as shown in Figure 5. Referenced to the middle of eclipse, the bright phase appears as a smooth "hump" lasting from $\varphi = 0.6$ to 0.3, i.e., commencing $\sim$0.1 in phase prior to the optical, but terminating at the same phase as the optical after the eclipse. The rise toward peak brightness in X-rays is also steeper than in the optical; indeed X-ray maximum occurs slightly ahead of eclipse, whereas the optical light doesn't peak until $\Delta\varphi \sim 0.1$ after eclipse. Within the uncertainties, the profiles of the bright phases and eclipses are consistent over the 2.4 cycles covered. Light curves extracted over different energy intervals (e.g., $0.1-0.6$ keV and $0.6-10$ keV) are strongly signal-to-noise ratio limited and do not provide useful information on hardness ratio changes over interesting phase intervals.

In the standard picture for Polars in their active accretion state ($\dot{m} \gtrsim 1$ g cm^{-2} s^{-1}) the X-ray emission is characterized by two components: (i) a hard ($kT \sim 10-30$ keV) thermal plasma component (e.g. bremsstrahlung) from the post-shock accretion column, and (ii) a soft, blackbody component from the underlying irradiated white dwarf photosphere. Theoretically, the reprocessed fraction of the total accretion energy is expected to be $L_{bb}/L_{acc} \sim 0.56$ (King & Watson 1987) . However, X-ray observations of Polars have often indicated a so-called "soft X-ray excess" (Ramsay et al. 1994), with the soft/hard ratio in excess of one, hence additional heating mechanisms have been proposed to enhance the relative contribution from the blackbody. The most widely accepted is the "bombardment" scenario, wherein the accretion funnel contains blobs of plasma of varying lengths/densities, the densest being able to penetrate beyond an optical depth of unity into the white dwarf before being shocked, effectively heating the atmosphere from below (Kuijpers & Pringle 1982).

We chose a single temperature bremsstrahlung model for the harder component, as the aim of this relatively short observation was to place constraints on the temperatures and hard/soft flux contributions. A joint fit of a blackbody plus thermal bremsstrahlung was performed on the three PN and MOS datasets within XSPEC[11]. The data were binned to give >30 counts per bin and χ^2 statistics were used to find the best overall fit to the background subtracted spectra. There remain uncertainties in the cross-calibration of the effective areas of the PN and MOS detectors, hence the model normalizations were allowed to differ. Fits attempted with both column density n_H and kT_{bb} as free variables were not well constrained, therefore fits were examined for typical values of $kT_{bb} = 20$, 30 and 40 eV, and n_H ranging from $0.5 - 2.7 \times 10^{20}$ cm^{-2}, the upper limit being the value given by the HEASARC column density tool[12], which estimates the column through the entire Galaxy for this sky position.

The reliability of the detector calibrations at the lowest energies is still unclear. We therefore used two sets of low energy cut-offs when fitting the spectra: i) energies >0.15 keV for PN and >0.2 keV for MOS, potentially useful for constraining any soft blackbody component, and ii) more conservative limits of $E > 0.3$ keV (PN) and >0.5 keV (MOS). Including the lowest energy bins we find equally good fits ($\chi^2_\nu = 1.1$, 101 degrees of freedom) with $n_H = 0.5 - 1.0 \times 10^{20}$ cm^{-2}, $kT_{br} = 8.0^{+1.6}_{-1.0}$ keV and any of the blackbody temperatures. However, only in the case of the coolest blackbody and $n_H = 1.0 \times 10^{20}$ cm^{-2} is the soft component required for the fit (an F-test yields a 98% confidence level, compared to $\ll 1\%$ for the other temperatures). This 20 eV blackbody contributes

[11] http://heasarc.gsfc.nasa.gov/docs/xanadu/xspec/index.html

[12] http://heasarc.gsfc.nasa.gov/cgi-bin/Tools/w3nh/w3nh.pl

1.1×10^{-12} erg cm^{-2} s^{-1} to the unabsorbed $0.01 - 10$ keV flux, while in all cases the bremsstrahlung component provides 2×10^{-12} erg cm^{-2} s^{-1}. On the other hand, if n_H is as high as 2.7×10^{20} cm^{-2}, for all blackbody temperatures the F-test gives confidence levels >95% for inclusion of the soft component, and the best fit is obtained for $kT_{bb} = 40$ eV and $kT_{br} = 6.7 \pm 0.8$ keV. This fit, which also yields $\chi^2_\nu = 1.1$ for 101 d.o.f., is shown in Figure 6. Again the bremsstrahlung flux is 2×10^{-12} erg cm^{-2} s^{-1}, with the blackbody adding a further $0.6 - 26 \times 10^{-12}$ erg cm^{-2} s^{-1} for the $40 - 20$ eV temperatures, respectively. The more conservative lower limits do not lead to a constraint on the blackbody component at all. This is almost certainly a consequence of losing the information below 0.3 keV. For a thermal bremsstrahlung component alone we find temperatures of 7.8 ± 1.0 and 6.5 ± 0.8 keV for column densities of 0.7 and 2.73×10^{20} cm^{-2}, respectively, with the same flux as above.

Accounting for geometrical effects, the X-ray scattering albedo of the white dwarf photosphere, $a_x = 0.3$ (Williams, King, & Brooker 1987), and neglecting the cyclotron term (usually an order of magnitude smaller than the bremsstrahlung component) gives luminosities of $L_{bb} \approx \pi F_{bb}(1 - a_x)d^2$ and $L_{acc} \approx L_{br} = 2\pi F_{br}(1 + a_x)d^2$, where d is the distance. This leads to a soft/hard luminosity ratio of $0.1 - 3.5$ for the higher n_H value ($kT_{bb} = 40 - 20$ eV) or $0 - 0.15$ for the lower values of n_H. It seems more likely that column density lies in the range $1.0 - 2.7 \times 10^{20}$ cm^{-2}, as the absence of a soft component is difficult to explain given an active accretion state at the time.

The low ratio of soft/hard X-ray luminosity is as expected for the standard radial accretion model for Polars, although we cannot rule out a soft X-ray excess if the blackbody is sufficiently cool. Indeed, the most recent synopsis of *XMM* results on 21 magnetic systems by Ramsay and Cropper (2004) has cast doubt on the existence of the soft X-ray excess among Polars in general. Calibration issues as discussed above complicate a good determination for the soft components, and corrections must be made for reflection of the hard X-rays, optical thickness, and the contributions from the cyclotron emission. With these considerations in mind, we conclude that SDSS J0155+0028 is not unusual among Polars from an X-ray standpoint.

4. A SHORT-PERIOD MAGNETIC CV WITH WIDE VARIATIONS IN ACCRETION RATE

4.1. *Orbital Ephemeris*

Optical photometry of SDSS J0155+0028 by Woudt et al. (2004) led to a determination for the orbital period of 87.13 ± 0.02 min, or 0.060507(14) d. Here, the numbers in parentheses indicate the uncertainty in the final digits. We have combined the results of Woudt et al. with the eclipse timing of Dubkova et al. (2003) and the new X-ray and optical timings reported here. Table 2 summarizes all 19 eclipses spanning more than a year, with times of mid-eclipse shown as heliocentric Julian dates (HJD). The measurements are distributed such that a common orbital ephemeris can be derived without cycle-count ambiguity. The result, weighted by the estimated uncertainties of individual timings, and referenced to the second eclipse observed on 2002 December 5, is

$$\mathrm{HJD} = 2452613.78907(11) + 0.06051621(4) \cdot E \qquad (1)$$

For convenience, the cycle count appropriate to each eclipse is also listed in Table 2, and an "O-C" (observed minus computed) diagram is shown for the eclipse timings in Figure 7. The period is 2.7 min shorter than that of the previously shortest-period Polar, DP Leo. The accuracy of the ephemeris is sufficient to phase future observations of SDSS J0155+0028 to better than $\Delta\varphi = 0.05$ for a decade.

4.2. *Changes with Accretion State*

The sharp contrast in spectral properties between high and low accretion states of SDSS J0155+0028 is illustrated by excerpts from the time series spectropolarimetry shown as the bold curves in the top and bottom panels of Figure 8, respectively. Both panels represent the system soon after maximum light ($\varphi = 0.1$).

The high state in 2002 December is distinguished by a very blue continuum and emission-line spectrum showing H, He I, and He II lines, with the Balmer decrement Hα : Hβ : Hγ inverted and $F_{\lambda 4686} \approx F_{H\beta}$. The line ratios are characteristic of an accretion funnel in a highly active system, and any line emission component from the inner hemisphere of the heated secondary cannot be resolved in these low-resolution data. Cyclotron emission harmonics in the high state are indistinct, but peaks can be recognized near 5600Å, 6550Å, and 7600Å. The circular polarization is weak: +3% overall, increasing mildly to the blue. By contrast, the low-state flux spectrum from 2004 February displayed in the bottom panel is roughly flat in F_λ and shows emission lines that have faded in approximate proportion to the continuum. He I emission is nearly absent and $F_{\lambda 4686} < F_{H\beta}$. A rich spectrum of well-defined cyclotron features is evident in the low state, with peak wavelengths at ∼5180Å, 5590Å, 6210Å, 6860Å, and 7780Å. The net circular polarization increases monotonically from only a few per cent at the long-wavelength extreme to nearly 25% in the blue.

It is straightforward to interpret the highly structured, strongly polarized continuum in the low state as cyclotron emission from primarily a single accretion spot. Fitting the peak wavelengths in the above list to the formula for cyclotron emission in a single-temperature plasma (Cropper et al. 1988; Wickramasinghe 1988) results in the assignment of harmonic numbers $m = 10 - 6$, respectively, a magnetic field strength in the spot of 29 MG, and a temperature factor $kT \sin^2\theta = 15$ keV. The increase in polarization with frequency is a natural result of the rapid decline in cyclotron absorption coefficient with increasing harmonic number (Chanmugam et al. 1989). Note that even though we characterize 2004 Feb. as a low state, the optical depth at $m = 6$ (7800Å) is still high enough to quench the circular polarization, the harmonics overlap considerably, and the accretion column is optically thick in the Balmer series. Indeed, the flux spectrum in the bottom panel of Figure 8 is reminiscent of the low-state spectrum of VV Puppis ($B \sim 30$ MG; Wickramasinghe & Visvanathan 1979), where the accretion rate has been estimated to be at least an order of magnitude higher than for chronically anemic Polars like SDSS J1553+5516 ($<10^{-13}$ $M_\odot$ yr^{-1}; Szkody et al. 2003).

With an order of magnitude increase in brightness and circular polarization that is of the same sign but much reduced in amount, it would appear that the 2002 Dec. high state of SDSS J0155+0028 could be explained simply by optically-thick emission from an increased mass transfer rate onto the same magnetic pole. However, the diffuse cyclotron emission bumps evident at this epoch are more widely spaced, indicative of the addition of a second active accretion spot with a different field strength. Unfortunately, only three diffuse harmonics do not lead to a definitive solution, but the best fit occurs for an assignment of $\lambda\lambda$5600, 6550, 7600, to $m = 6, 5, 4$ respectively, $B \sim 48$ MG, and $T \sin^2\theta \sim 30$ keV. This suggests that the reduction in polarization in the high state may be due, in part, to the competition of two emission regions with opposite polarity. Simultaneous visibility of two accretion spots with unequal field strengths could arise if they represent complementary footpoints of closed field lines in an offset dipolar structure (e.g., Wickramasinghe, Ferrario, & Bailey 1989).

4.3. *System Parameters*

The eclipse duration in SDSS J0155+0028 has not yet been measured with high precision (our best time resolution is 10 s in the NOT observations). Nevertheless, available estimates permit useful checks on key parameters of the binary. For example, the generally high level of activity suggests that the secondary star fills its Roche lobe, which for a binary with $P = 87$ min implies a radius $R_2 = 0.14\ R_\odot$ (e.g., Pringle & Wade 1985). The maximum predicted eclipse length of an emission region on the white dwarf (as seen by an observer in the plane of the orbit) is a function of white dwarf mass, ranging from 460 to 380 s for $M_1 = 0.4$ to 0.8 $M_\odot$, respectively. Estimates for SDSS J0155+0028 range from ∼320 s (Woudt et al. 2004) to ∼390 s for our *XMM* data. Because a non-central eclipse reduces the duration of totality, these values favor the lower end of the mass range. If the secondary has the structure of a main-sequence star (questionable given the advanced age of this binary, but see Beuermann et al. 1998), it has a mass $M_2 = 0.11\ M_\odot$ (Beuermann & Weichhold 1999), an absolute visual magnitude $M_V \sim 15.1$ (Baraffe et al. 1998), and a spectral type of M5.5 (Henry, Kirkpatrick, & Simons 1994). A distance estimate is then possible by scaling the weak rise in spectral flux beyond $\lambda = 7000$ Å that is evident when the accretion spot is hidden from view to library flux spectra for M dwarfs. The best data for this purpose come from the low-state, faint-phase ($\varphi = 0.38$) MMT spectrum shown in the bottom panel of Figure 8, and we use for comparison the M dwarf standards that have been placed on an absolute magnitude scale in Sloan bands by (Hawley et al. 2002). We find $D \sim 290$ pc, with an uncertainty of at least 25%. However, even this crude estimate yields reasonable numbers for a Polar in an active accretion state (cf. Warner 1995): a $0.01 - 10$ keV luminosity of $L_X \sim 2 \times 10^{31}$ ergs s^{-1} and an accretion rate $\dot{M} > 4 \times 10^{-12}\ M_\odot$ yr^{-1}, the inequality resulting from the likelihood that cyclotron emission and the largely unmeasured soft X-ray component carry a significant fraction of the accretion luminosity. Compared with the several dozen Polars that have been studied over the past three decades, it appears that SDSS J0155+0028 is largely unremarkable except for an unusual viewing perspective, as discussed below.

5. ABSORPTION IN THE ACCRETION FUNNEL

Eclipse profiles are rich sources of information on the locations, sizes, and properties of emission regions in magnetic CVs. The overall duration of eclipse reflects the chord executed by the white dwarf and accretion spot(s) across the secondary star, and for a typical geometry lasts $\Delta\varphi \sim 0.08$. Ingress and egress of the white dwarf disk each require at least 30 s, depending on primary star mass, orbital period, and inclination, and appear most prominently in the near-UV (Schmidt & Stockman 2001). In the optical, the white dwarf is usually overwhelmed by the combination of the tiny accretion spot(s) (e.g., Bailey & Cropper 1991; Schwope et al. 2001) and continuum emission from the funnel, each of which provides a characteristic eclipse signature (e.g., Stockman & Schmidt 1996). The accretion stream can also be detected through absorption dips preceding primary eclipse in the emission lines and EUV (Schwope et al. 2001). For SDSS J0155+0028, the photometric database stands to be improved in both wavelength coverage and time resolution, but the eclipse depth ($m_V \sim 20$ at minimum) implies that a large telescope will be required.

Despite the limitations of available data, new information on the properties of the accretion stream in the high state – including the origin of the line absorption phase described by Szkody et al. (2002) – is available from our complete orbit of spectrophotometry obtained at the 2.3 m telescope in 2002 December. In Figure 9 we display the radial velocity and flux in the Hα emission line as a function of orbital phase for all phases where the line is uncontaminated by absorption. The results confirm that the accretion stream and funnel are the dominant sources of line emission in this state. Not only are the γ velocity and line widths very large (+200 km s^{-1}; 1000−1500 km s^{-1}, respectively), but the velocity curve is somewhat triangular, shows maximum redshift near the time of eclipse, and the line flux possesses two minima: one at eclipse ($\varphi = 0$) and a second 0.5 orbit later. All of these are characteristics of optically-thick emission in a flow that is directed largely along the line of sight near the stellar conjunctions.

The spectral sequence for the interval around eclipse is presented as Figure 10. Phase proceeds downward as marked, in intervals of 2.6 min (∼11° of orbital motion). The initial two spectra, taken at $\varphi = 0.82$ and 0.85, show strong Balmer, He II, and He I emission lines typical of active AM Her systems. The lines at this phase are approaching maximum redshift and are marginally resolved with a full width at half-maximum (FWHM) of ∼1000 km s^{-1}. At $\varphi = 0.88$, 40° prior to the primary mid-eclipse, the lines suddenly fade and P-Cygni type absorption components develop ∼450 km s^{-1} to the blue of the emission peaks in all lines *except* He II λ4686. By $\varphi = 0.91$ (30° prior to mid-eclipse), the absorption features have deepened and shifted redward to completely consume the emission lines. This is the phase of the photometric dip discussed in §2. The prominence of the dip in B and R (Figure 3) as opposed to V reflects the presence of Hβ and Hα in the two former filter bands. Resuming the time series, the absorption lines narrow to ∼800 km s^{-1} FWHM

and continue to shift some 400 km s^{-1} to the red before the P-Cygni phase returns at $\varphi = 0.97$. Following this, the system quickly drops into the deep primary eclipse. This transformation is better displayed in an enlarged version of the phase interval shown as Figure 11.

At mid-eclipse, the emission lines are reduced in brightness by about an order of magnitude. The weak continuum has $m_V \sim 20$ and exhibits a somewhat concave appearance. Because the white dwarf is eclipsed, the continuum at this time is probably bound-free and free-free emission (e.g., Kim & Beuermann 1996) plus possibly scattered cyclotron emission from the portion of the accretion stream and funnel that is still visible. Eclipse egress occurs over the course of $\Delta\varphi \sim 0.06$ ($\Delta\theta \sim 20°$), with full exposure of the line-emitting funnel lagging the continuum.

We recognize the development of P-Cygni components followed by full absorption reversals of the lines for $0.88 < \varphi < 0.97$ as a self-eclipse of the accretion funnel, a rare opportunity afforded by our fortuitous viewpoint of SDSS J0155+0028. Only EF Eri (Verbunt et al. 1980) and MN Hya (Ramsay & Wheatley 1998) have shown this effect, and then in only a few lines. The geometry for SDSS J0155+0028 is depicted in the sketch shown as Figure 12. Here, the Earth lies in the plane of the paper, with the observer orbiting the binary in a clockwise direction. The stellar components are shown to scale for an assumed 0.6 $M_\odot$ white dwarf and Roche-lobe filling secondary. Also indicated is the ballistic stream trajectory and viewing phases corresponding to the spectra displayed in Figure 10. The shaded area in the figure is a schematic representation of the accretion funnel that is consistent with the observations. In order that a self-eclipse occurs, the funnel must terminate in one or more accretion spots not far from the white dwarf equator. The azimuth range of the funnel has been estimated from the duration of the absorption-line phase, but we also note that with this geometry, full exposure of the stream following primary eclipse of the white dwarf would not occur until nearly $\varphi = 0.1$, as observed. The inference from this sketch is that the dominant magnetic pole lies at a longitude of $\psi \approx +30°$, i.e., that it leads the secondary in its orbit. This is supported by the folded X-ray light curve in Figure 5, where it can be seen that the onset and conclusion of the bright phase are displaced around the deep eclipse by $\Delta\varphi \approx -0.1$.

It was realized early in the studies of AM Herculis (Stockman et al. 1977) that the high-state emission lines of Polars are formed in dense ($N_e \gtrsim 10^{13}$ cm^{-3}), collimated inflows that are optically thick in the permitted lines. Heating to temperatures of ∼10,000−40,000 K is provided largely by hard and soft X-ray irradiation from the vicinity of the shock, with the temperature generally falling with radial distance (e.g., Ferrario & Wickramasinghe 1993). It is therefore not surprising that the lines could be seen in absorption if the funnel were viewed through its cool, upper end. However, models of the emission lines in mCVs constructed by Ferrario & Wehrse (1999) found that, while radiative heating alone can account for the Balmer lines, it is insufficient to explain the strengths of He I and He II lines. The large volume present in the coupling region – where the gas attaches to the white dwarf's magnetic field lines – offered an attractive alternative site for the origin of the helium features, but an additional source of heating was required. Magnetic turbulence and reconnection, or weak shocks were suggested as candidate mechanisms. These ideas make certain predictions that can be tested with our observations of SDSS J0155+0028.

Referring again to Figure 11, we note first that the H and He I lines behave similarly through the spectral sequence, indicating no qualitative difference in their origins. Given the contrasting behavior of He II λ4686 (see also below), this is already at odds with the predictions of Ferrario & Wehrse (1999). P-Cygni absorption components initially appear in the blue wings of the Balmer and He I lines, confirming that the foreground gas is both cooler and receding with a smaller velocity than what causes the bulk of the line emission. This situation is reproduced at the termination of self-eclipse near $\varphi = 0.97$. As the funnel self-eclipse progresses, absorption components deepen and move toward redder wavelengths. The fact that the phase of maximum line depth ($\varphi \approx 0.9$) coincides with our most face-on view of the accretion spot indicates that the funnel is primarily radial, as indicated in Figure 12. It is interesting, however, that the absorption components completely consume the emission lines. Indeed, the line width (FWHM $\approx$ 1400 km s^{-1} at maximum depth) appears to exceed that of the preceding emission lines (∼1000 km s^{-1}). This might be understood if the funnel temperature increases not only as one moves toward the white dwarf, but also from the funnel core to surface. Such a profile would, of course, result from radiative heating from below. A sight-line through the shielded funnel base, such as we are afforded at $\varphi = 0.9$, would then view comparatively cool gas projected against the hot funnel skin over the full range of radial velocities, and very broad absorption lines would result. The sketch for SDSS J0155+0028 shown in Figure 12 corresponds closely with a similar diagram showing an accretion curtain and vertical stream in HU Aqr (Schwope, Mantel, & Horne 1997).

The progressive shift of the absorption features to higher velocity through the funnel eclipse phase is more puzzling, given the simple geometry sketched in Figure 12. Certainly gas that attaches to field lines early in its journey (and so appears in absorption late in the sequence) does so onto paths that are more closely aligned with their original ballistic stream trajectories; this gas might therefore preserve a higher fraction of its infall velocity. Alternatively, the gas density might vary with azimuth in such a way that we see more deeply into the funnel at later eclipse phases, thus absorption appears at higher redshift at these times. Additional spectroscopy with both higher time and velocity resolution would help to clarify among the possibilities.

The He II λ4686 emission line is nearly stationary in wavelength and largely unchanged in brightness through the funnel self-eclipse, the largest effect being the formation of a brief and weak P-Cygni component at the phase of maximum absorption-line depth. These properties are consistent either with the funnel being essentially optically thin in λ4686, and/or with the emission line being produced primarily in a coupling region high above the white dwarf, as Ferrario & Wehrse (1999) suggest. We note that the high-state data shown in Figures 10 and 11 were obtained with a 2.3 m telescope, so better quality and resolution are not only desirable but practical.

6. SUMMARY AND CONCLUSIONS

With a period of 87.13 min, SDSS J0155+0028 is the shortest-period eclipsing Polar known. Observations to date indicate that the system is highly active ($m_V = 15 - 16$) a large fraction of the time, and reveal an X-ray light curve and spectrum, as well as a low-state optical cyclotron emission spectrum, that are characteristic of active Polars ($kT \sim 10$ keV; $B \sim 30$ MG). The >5 mag deep, ∼6.5 min duration eclipse has yielded an accurate ephemeris, but photometry with higher time resolution and spectrophotometry with better spectral resolution will provide a more detailed understanding of the stellar components, the extent of the funnel, and the accretion spot location(s) on the white dwarf surface. Particularly interesting is an absorption-line phase that immediately precedes the main eclipse. This is interpreted as the result of a favorable viewing perspective of the optically-thick accretion flow through the cool base of the funnel, which must lie virtually in the plane of the orbit. Existing observations have yielded a simple description of the gas flow, but future high-quality spectrophotometry through the absorption-line phase promises to be a powerful technique for mapping the trajectory and properties of the accretion flow in this magnetic CV.

The authors thank P. Woudt for sharing his photometry in advance of publication. GDS is grateful to the Director of Steward Observatory for funding the foundry run of STA devices, from which an improved CCD for the spectropolarimeter was obtained, and to M. Lesser for optimizing the chip for astronomy. The anonymous referee offered several useful suggestions and corrections to an earlier version of the manuscript. Support was provided by NASA through *XMM* Grant NAG5-12938 and the NSF through AST 03-06080. JES acknowledges support by the "Access to the ENO" project 02-038 from the European Union. This work is based, in part, on observations obtained with *XMM-Newton*, an ESA science mission with instruments and contributions directly funded by ESA Member States and the USA (NASA). Part of the optical data were taken using ALFOSC, which is owned by the Instituto de Astrofisica de Andalucia (IAA) and operated at the Nordic Optical Telescope under agreement between IAA and the NBIfAG of the Astronomical Observatory of Copenhagen.

REFERENCES

Bailey, J., & Cropper, M. 1991, MNRAS, 253, 27
Baraffe, I., Chabrier, G., Allard, F., & Hauschildt, P.H. 1998, A&A, 337, 403
Beuermann, K., & Weichhold, M. 1999, in ASP Conf. Ser. 157, Annapolis Workshop on Magnetic Cataclysmic Variables, ed. C. Hellier & K. Mukai (San Francisco: ASP), 283
Beuermann, K., Baraffe, I., Kolb, U., & Weichhold, M. 1998, A&A, 339, 518
Chanmugam, G., Wu, K., Courtney, M.W., & Barrett, P.E. 1989, ApJS, 71, 323
Cropper, M., Mason, K.O., Allington-Smith, J.R., Branduardi-Raymont, G., Charles, P.A., Mittaz, J.P.D., Mukai, K., Murdin, P.G., & Smale, A.P. 1988, MNRAS, 236, 29P
den Herder, J. W., et al. 2001, A&A, 365, L7
Dubkova, D.N., Kudryavtseva, N.A., & Hirv, A. 2003, IBVS 5389
Ferrario, L., & Wehrse, R. 1999, MNRAS, 310, 189
Ferrario, L., & Wickramasinghe, D.T. 1993, MNRAS, 265, 605
Hawley, S.L., et al. 2002, ApJ, 123, 3409
Henry, T.J., Kirkpatrick, J.D., & Simons, D.A. 1994, AJ, 108, 1437
Kim, Y., & Beuermann, K. 1996, A&A, 307, 824
King, A. R., & Watson, M. G. 1987, MNRAS, 227, 205
Kuijpers, J., & Pringle, J. E. 1982, A&A, 114, L4
Mason, K. O., et al. 2001, A&A, 365, L36
Pringle, J.E., & Wade, R.A. 1985, Interacting Binary Stars, (Cambridge: Cambridge University Press), pp. 198-199
Ramsay, G., & Cropper, M. 2004, MNRAS, 347, 497
Ramsay, G., Mason, K. O., Cropper, M., Watson, M. G., & Clayton, K. L. 1994, MNRAS, 270, 692
Ramsay, G., & Wheatley, P.J. 1998, MNRAS, 301, 95
Reimers, D., & Hagen, H.-J. 2000, A&A, 358, L45
Reimers, D., Hagen, H.-J., & Hopp, U. 1999, A&A, 343, 157
Ritter, H., & Kolb, U. 2003, A&A, 404, 301
Schmidt, G.D., Ferrario, L., Wickramasinghe, D.T., & Smith, P.S. 2001, ApJ, 553, 823
Schmidt, G.D., & Stockman, H.S. 2001, ApJ, 548, 410
Schmidt, G.D., Stockman, H.S., & Smith, P.S. 1992, ApJ, 398, L57
Schmidt, G.D., Szkody, P., Smith, P.S., Silber, A., Tovmassian, G., Hoard, D.W., Gänsicke, B.T., & de Martino, D. 1996, ApJ, 473, 483
Schwope, A.D., Mantel, K.-H., & Horne, K. 1997, A&A, 319, 894
Schwope, A.D., Schwarz, R., Sirk, M., & Howell, S.B. 2001, A&A, 375, 419
Stockman, H.S. 1988, in Polarized Radiation of Circumstellar Origin, ed. G.V. Coyne, A.F.J. Moffat, S. Tapia, A.M. Magalhaes, R. Schulte-Ladbeck, & D.T. Wickramasinghe (Tucson: Univ. of Arizona Press), 237
Stockman, H.S., & Schmidt, G.D. 1996, ApJ, 468, 883
Stockman, H.S., Schmidt, G.D., Angel, J.R.P., Liebert, J., Tapia, S., & Beaver, E.A. 1977, ApJ, 217, 815
Szkody, P., et al. 2002, AJ, 123, 430
Szkody, P., et al. 2003, ApJ, 583, 902
Turner, M., et al. 2001, MNRAS, A&A, 365, L27
Verbunt, F., van den Heuvel, E.P.J., van der Linden, T.J., van Paradijs, J., Brand, J., & van Leeuwen, F. 1980, A&A, 86, L10
Warner, B. 1995, Cataclysmic Variable Stars, (Cambridge: Cambridge Univ. Press), 343-347
Wickramasinghe, D.T. 1988, in Polarized Radiation of Circumstellar Origin, ed. G.V. Coyne, A.F.J. Moffat, S.Tapia, A.M. Magalhaes, R. Schulte-Ladbeck, & D.T. Wickramasinghe (Tucson: Univ. of Arizona Press), 199
Wickramasinghe, D.T., Ferrario, L., & Bailey, J. 1989, ApJ, 342, L35
Wickramasinghe, D.T., & Visvanathan, N. 1979, MNRAS, 191, 589
Williams, G. A., King, A. R., & Brooker, J. R. E. 1987, MNRAS, 226, 725
Woudt, P.A., Warner, B., & Pretorius, M.L. 2004, MNRAS, 351, 1015

TABLE 1
XMM-Newton OBSERVATIONS OF SDSS J0155+0028

Instrument	Date (yyyy-mm-dd)	UT	Exposure (s)	Counts s^{-1}
PN	2003-07-04	14:27−16:34	4920	0.0−1.00
MOS1	2003-07-04	13:13−16:37	12254	0.0−0.28
MOS2	2003-07-04	13:13−16:37	12264	0.0−0.34

TABLE 2
ECLIPSE TIMES FOR SDSS J0155+0028

Eclipse Center (HJD − 2450000)	Cycle	Source
2506.6751	−1770	1, NOT 2.56 m
2531.9713	−1352	2, MRO 0.76 m
2563.560	−830	2, NOT 2.56 m
2563.621	−829	2, NOT 2.56 m
2563.686	−828	2, IAC 0.6 m
2592.544	−351	2, IAC 0.8 m
2592.605	−350	2, IAC 0.8 m
2593.7586	−331	2, USNO 1.0 m
2593.8194	−330	2, USNO 1.0 m
2593.8788	−329	2, USNO 1.0 m
2613.7281	−1	2, SO 2.3 m
2613.7892	0	2, SO 2.3 m
2824.932	3489	2, USNO 1.0 m
2825.0513	3491	2, *XMM*
2825.1115	3492	2, *XMM*
2825.1717	3493	2, *XMM*
2825.960	3506	2, USNO 1.0 m
2917.3990	5017	3, SAAO 1.9 m
2918.4278	5034	3, SAAO 1.9 m

References. — [1]Dubkova et al. (2003); [2]This paper; [3]Woudt et al. (2004).

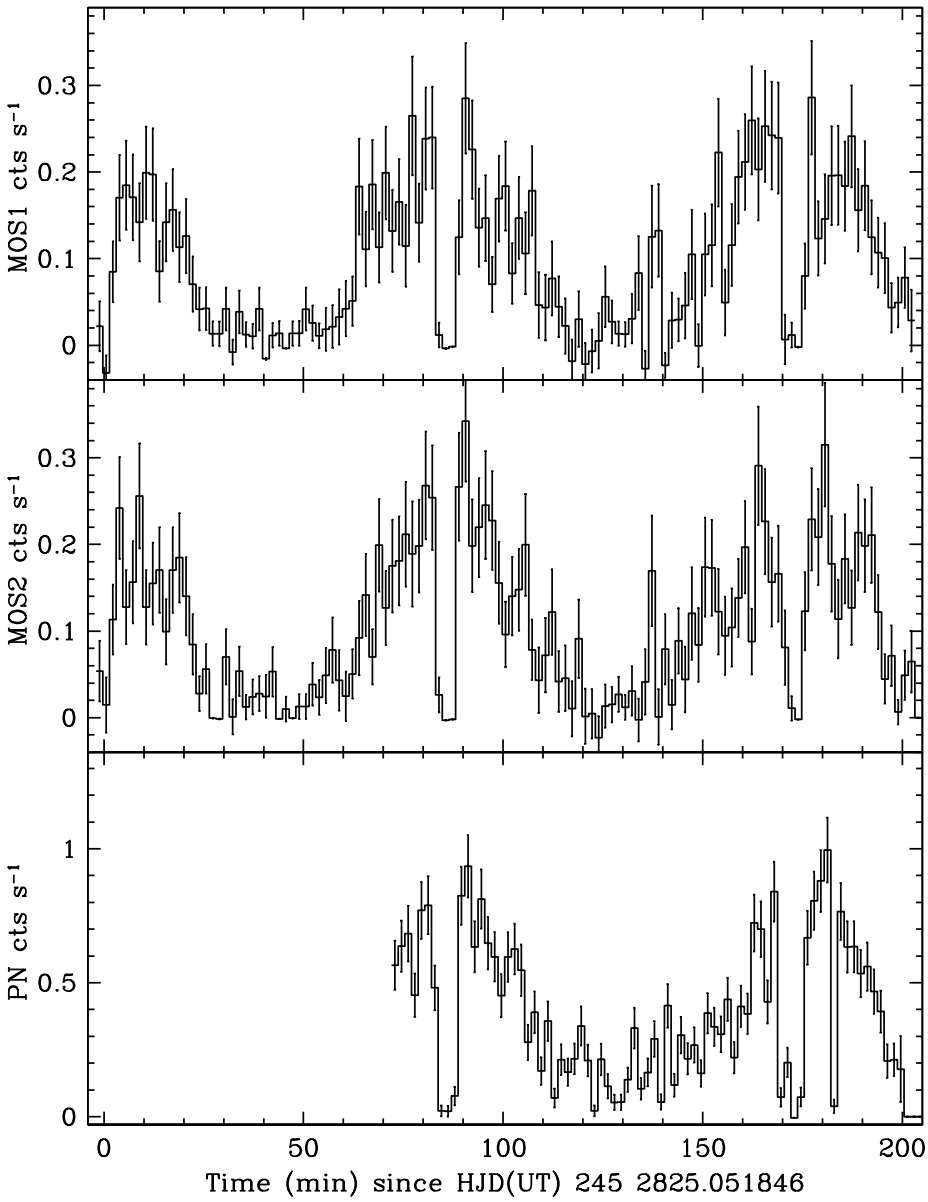

FIG. 1.— *XMM-Newton*/EPIC-pn and MOS time series with 100 s binning. Note the single-humped light curve characteristic of a one-pole accretor, punctuated by a total eclipse of duration ∼390 s. The latter half of the PN light curve was obtained as a large number of short exposures, so the exposure time per bin is nonuniform and occasionally very short.

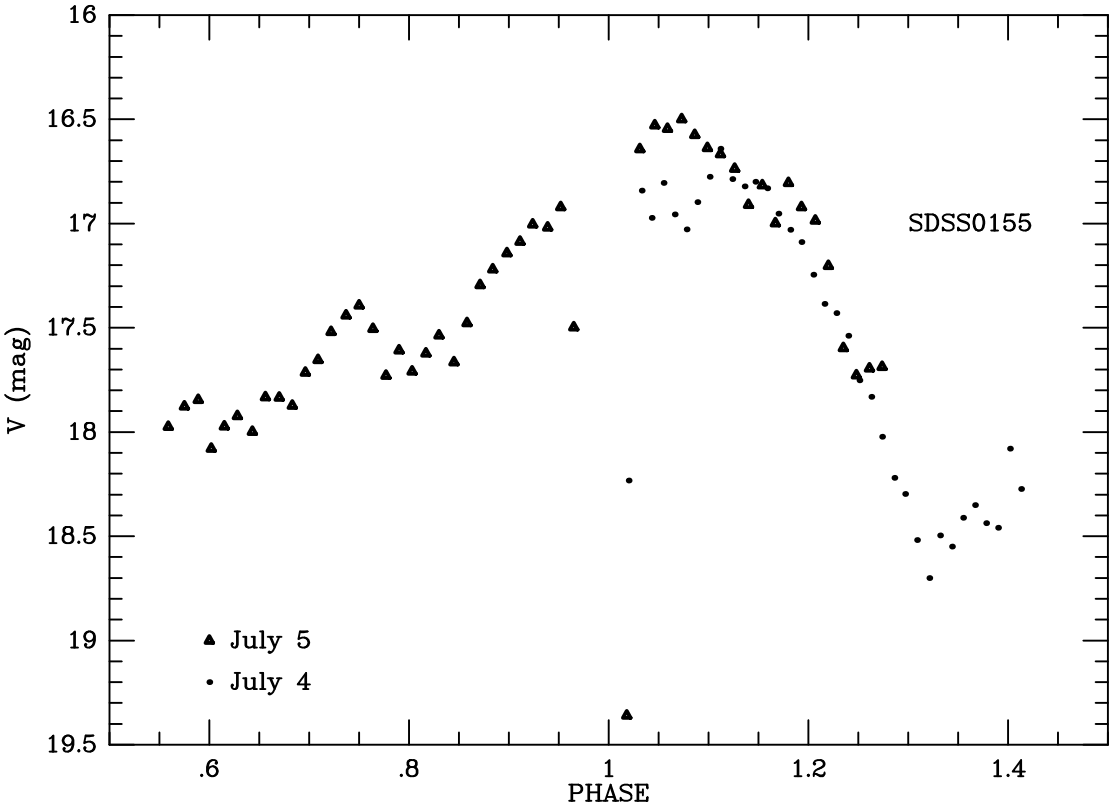

FIG. 2.— Optical photometry obtained on the nights immediately preceding (July 4 UT) and following (July 5 UT) the *XMM* observations, confirming that SDSS J0155+0028 was in an active accretion state for the X-ray measurements.

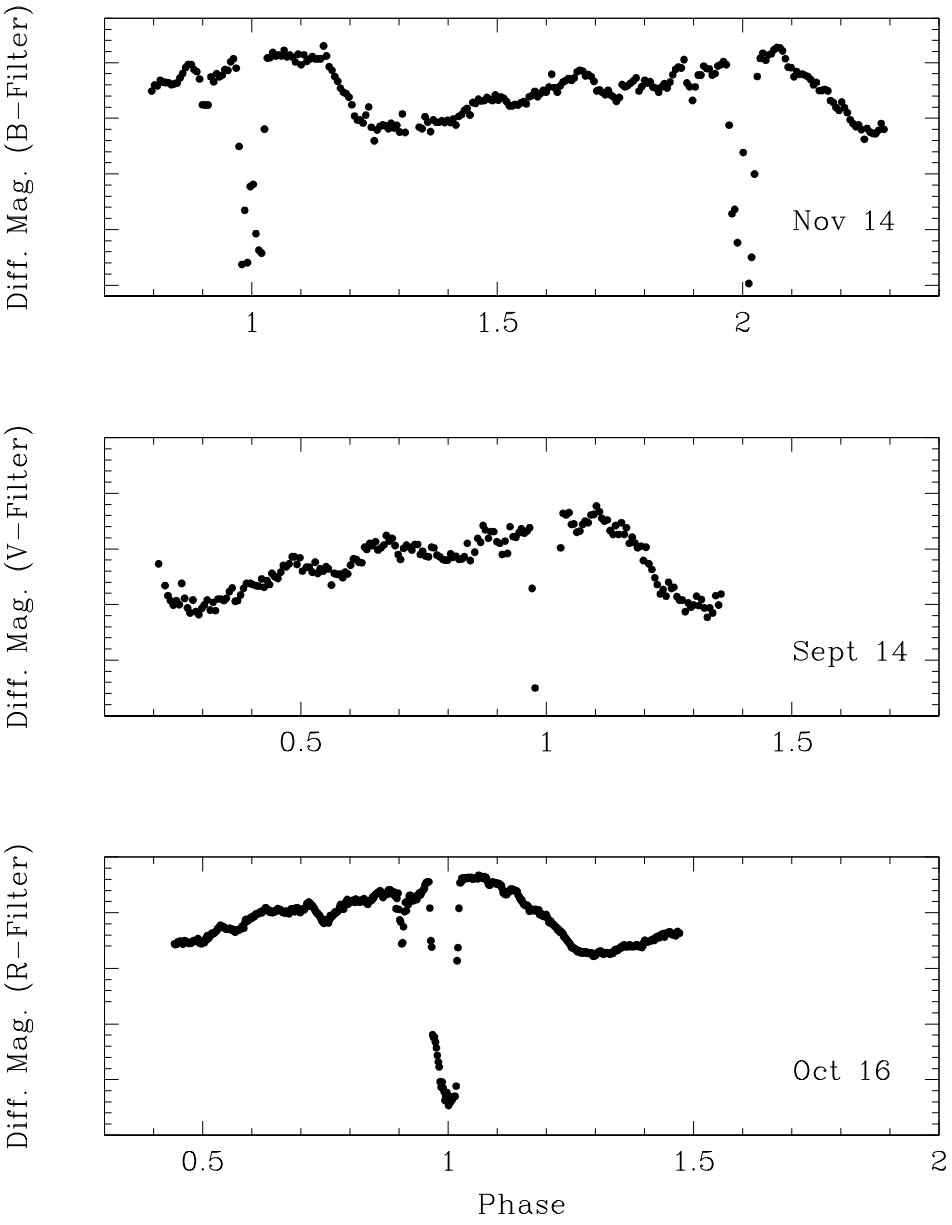

FIG. 3.— Differential photometry of SDSS J0155+0028 obtained during the high accretion state with various filters and telescopes in the fall of 2002. Note the brief dip near $\varphi = 0.9$ in each panel, suggestive of a stream eclipse. Each large interval on the ordinate represents a difference of one magnitude.

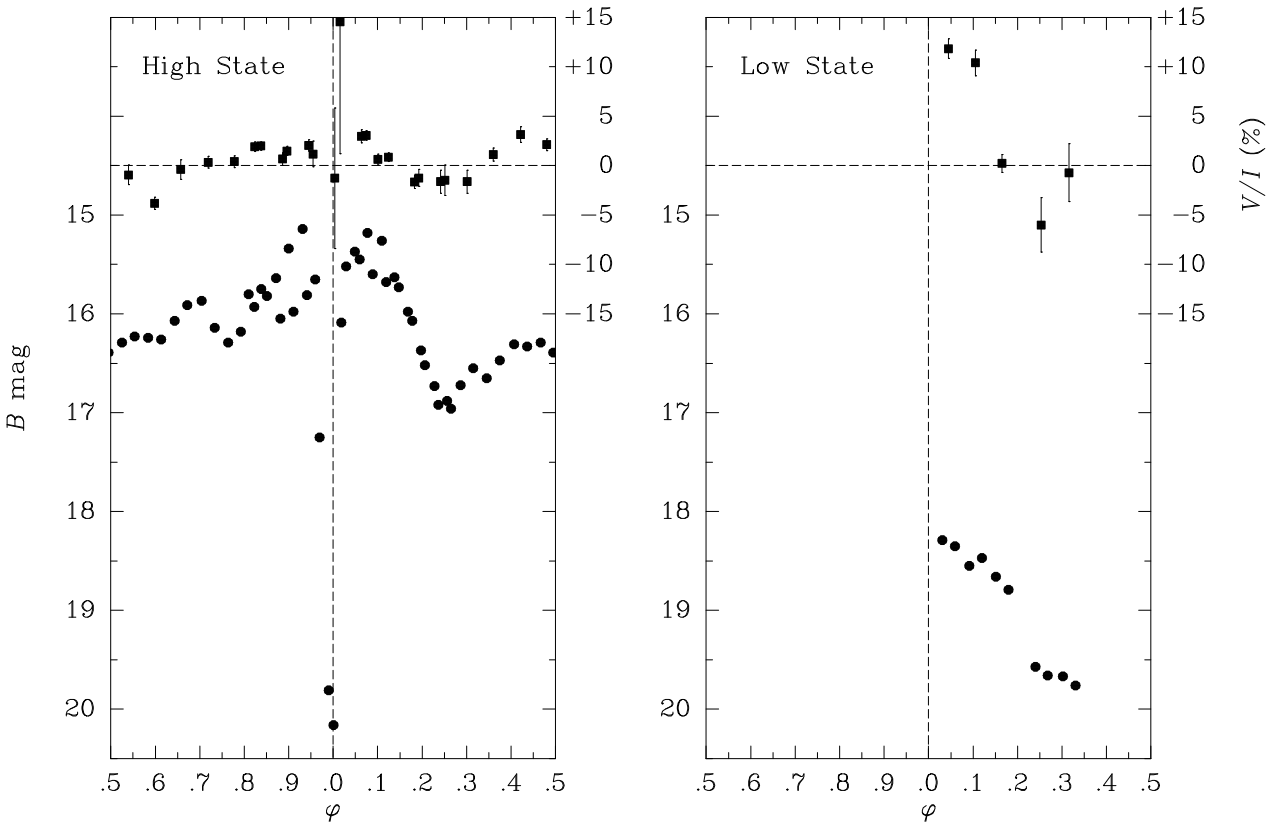

FIG. 4.— *(Left:)* Spectrum-added circular polarization in per cent *(squares)* and B-band brightness *(circles)* extracted from 1.5 orbits of spectropolarimetry obtained during a high state of SDSS J0155+0028 in 2002 Dec. The data are phase-folded on the ephemeris derived in §4.1. Note the weak polarization, which varies in sign through the cycle. *(Right:)* Results from a partial orbit acquired in a low accretion state in 2004 Feb. Circular polarization in the low state is large during the interval that the accretion spot is in view.

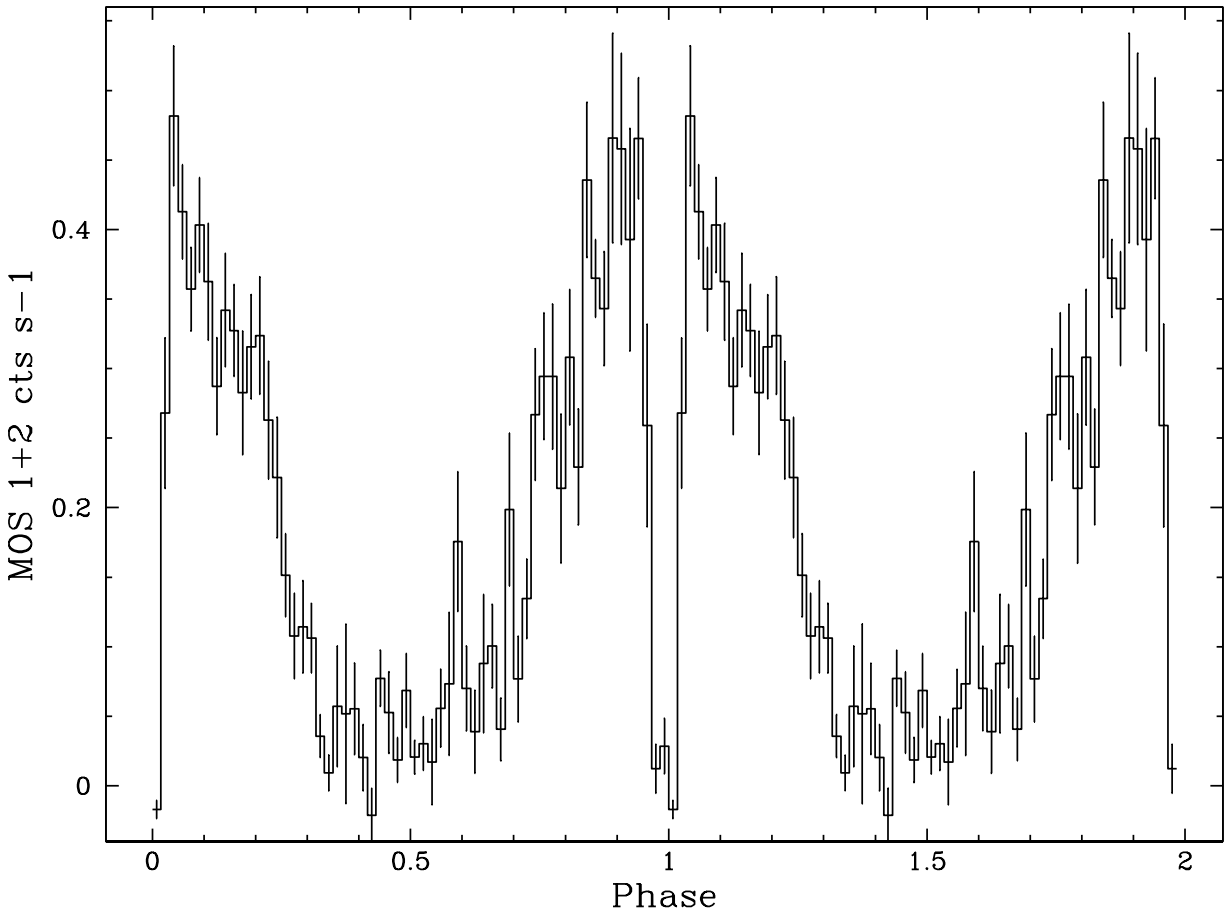

FIG. 5.— Mean light curve from the two *XMM-Newton*/EPIC-MOS cameras, folded using the ephemeris derived in §4.1.

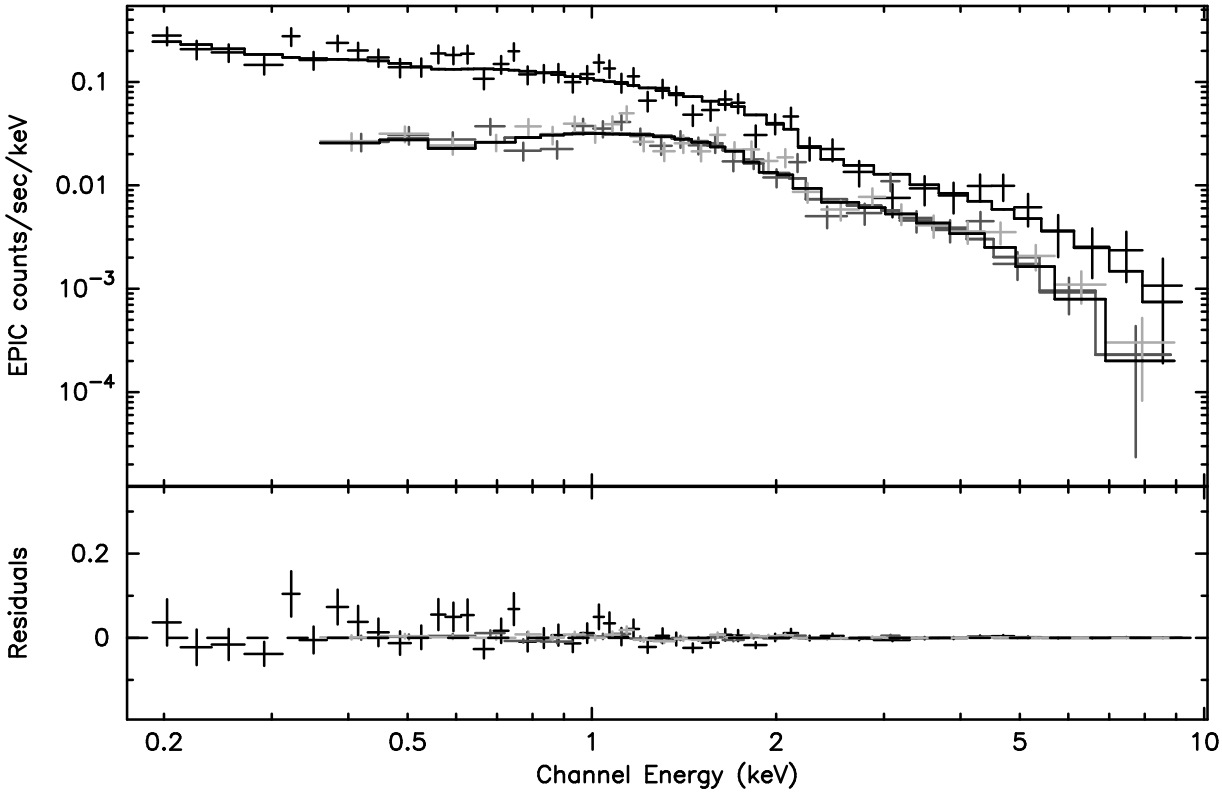

FIG. 6.— *XMM-Newton*/EPIC-pn *(upper)* and MOS *(lower)* spectra. The fit shown uses a 40 eV blackbody plus a 7 keV thermal bremsstrahlung component (overplotted lines), although the inclusion of the blackbody is not required at high significance. Residuals to the fit are shown in the lower panel.

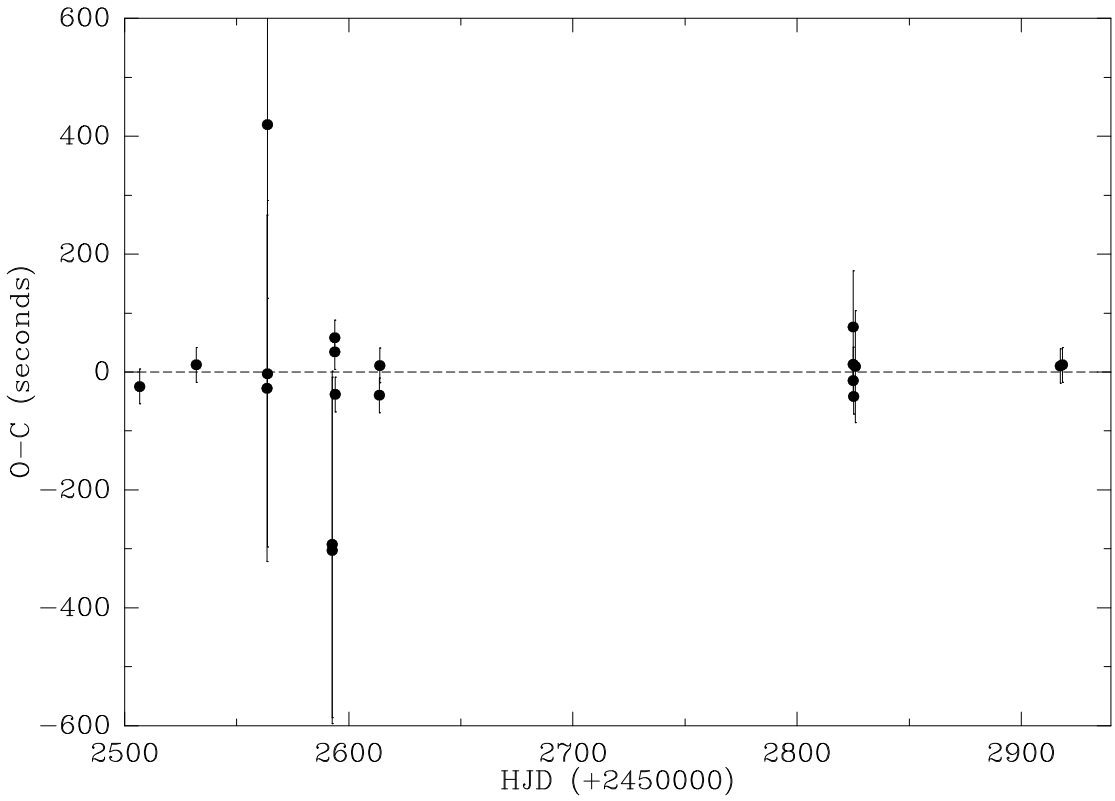

FIG. 7.— An "observed minus computed" diagram for all 19 eclipse timings of SDSS J0155+0028 (Table 2), using the ephemeris derived in §4.1.

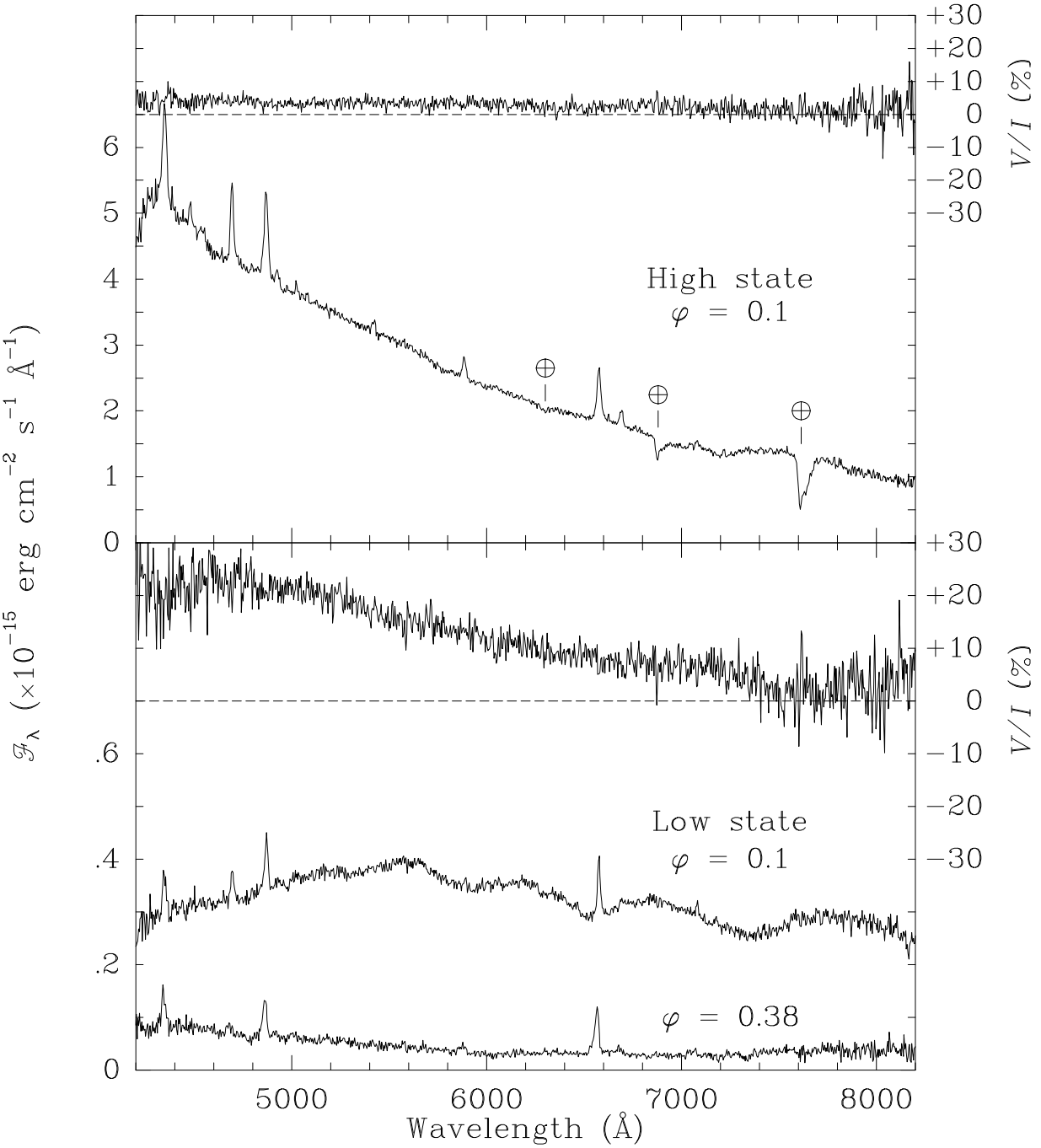

FIG. 8.— Comparison of total flux and circular polarization spectra of SDSS J0155+0028 for high ($m_V = 15.2$) and low accretion states ($m_V = 17.5$), both obtained soon after eclipse at $\varphi = 0.1$. The steep blue continuum, inverted Balmer decrement, and smeared cyclotron harmonics in the high state are indicative of a high-temperature shock, while the reduced polarization throughout the spectrum results at least in part from the increased cyclotron optical depth. Note also the more widely-separated harmonics in the high state; an indication of a second active pole. The additional low-state spectrum shown in the bottom panel represents the system when the active pole is self-eclipsed by the white dwarf, and shows a slight upturn in the red due to the cool companion star. Uncorrected terrestrial absorption in the upper panel are marked.

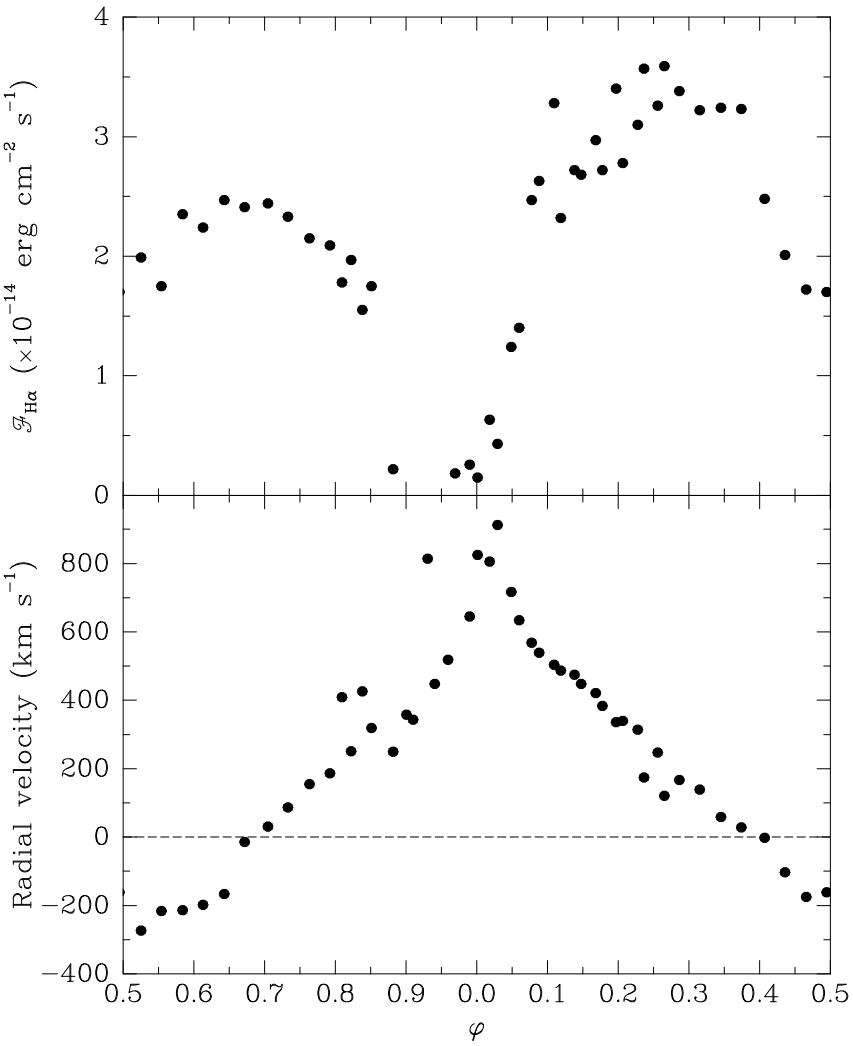

FIG. 9.— Radial velocity curve *(bottom)* and line flux *(top)* in Hα for the high state of 2002 Dec. Phases where the emission line is absent or contaminated by absorption have been omitted.

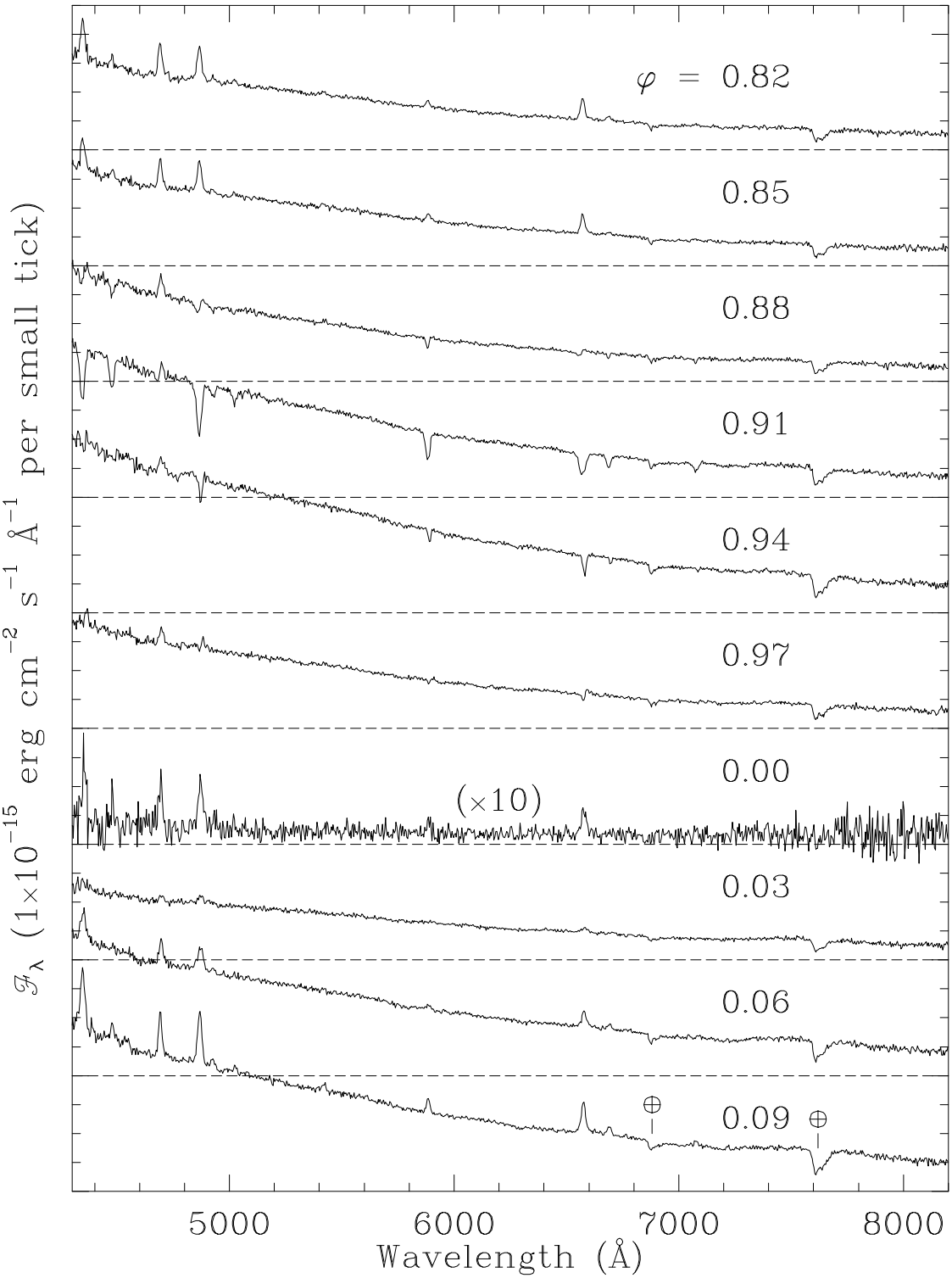

FIG. 10.— Spectral sequence through eclipse during the high state of SDSS J0155+0028. Time proceeds from top to bottom, with orbital phase indicated. Self-eclipse of the line-emitting stream begins at $\varphi = 0.88$ (40° prior to primary eclipse) with the development of weak P-Cygni profiles in the hydrogen Balmer and He I lines. This spectrum recurs just prior to ingress of the primary eclipse. Note that He II λ4686 never dips completely into absorption. Dashed lines indicate the zero-flux level of successive spectra.

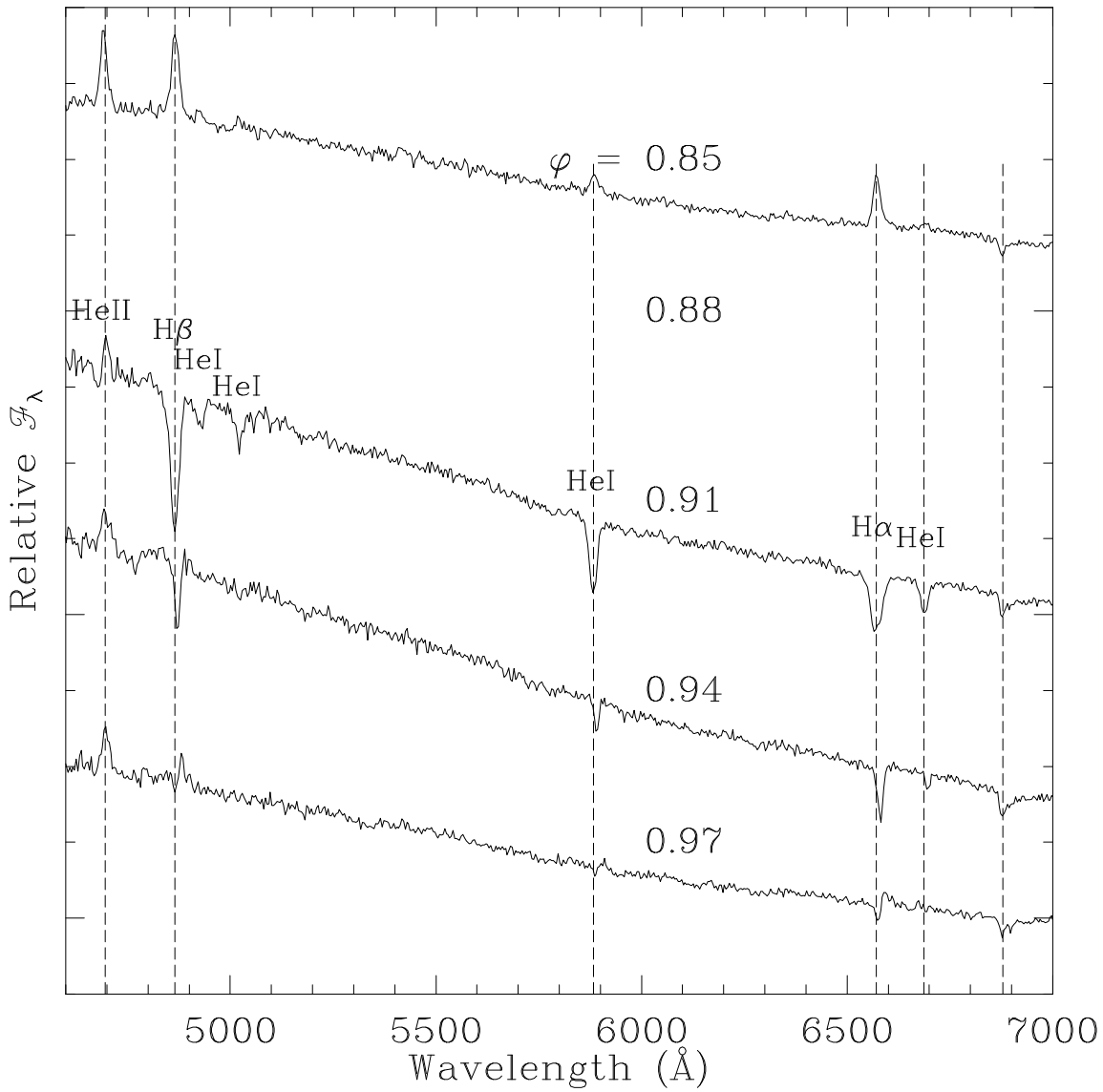

FIG. 11.— Enlarged view of the spectral sequence leading up to primary eclipse. Note the development of P-Cygni features, followed by deep absorption components for all lines except He II λ4686. The absorption lines, which reach 50% in depth for Hβ, become sharper and shift to the red as primary eclipse approaches. The stationary feature at 6884 Å is a terrestrial absorption bandhead of O_2.

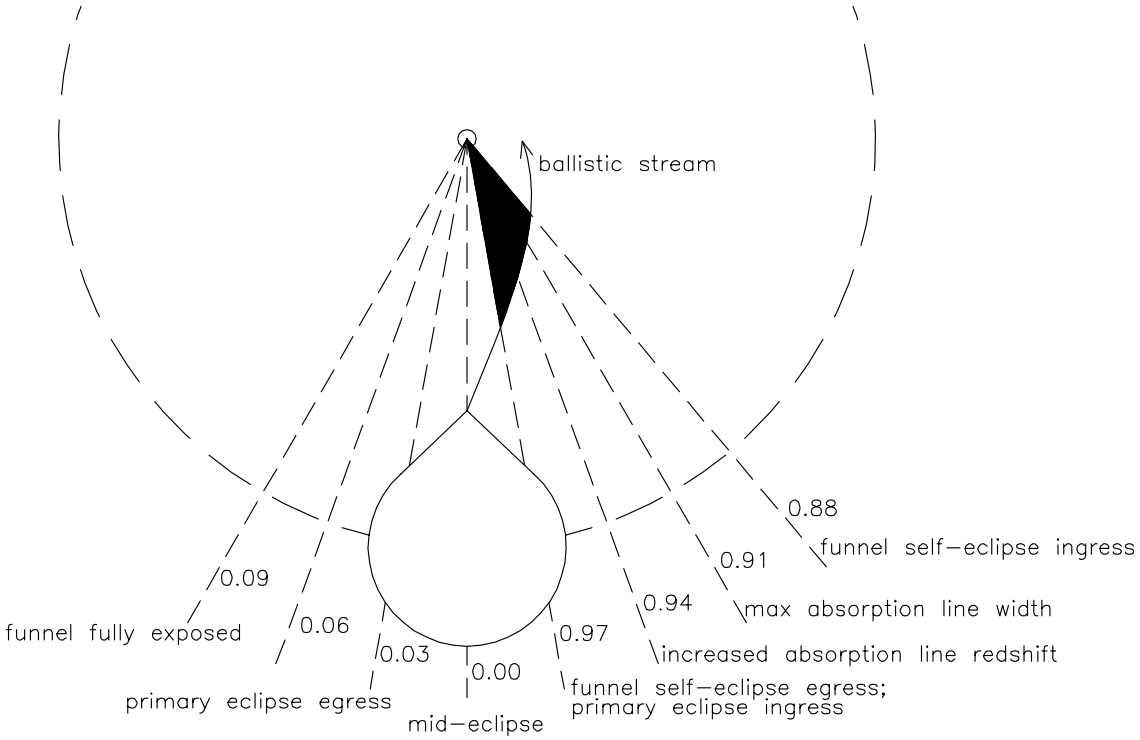

FIG. 12.— Sketch of SDSS J0155+0028, shown to scale for an assumed 0.6 $M_\odot$ white dwarf and Roche-lobe filling, main-sequence secondary ($M_2 = 0.11\ M_\odot$). The Earth lies very nearly in the orbital plane, with the observer orbiting the binary clockwise with phase. Also indicated is the ballistic stream trajectory projected onto the orbital plane and viewing phases corresponding to the spectra displayed in Figures 10 and 11.